

Effects of Laser Parameters on Porosity Formation: Investigating Millimeter Scale Continuous Wave Nd:YAG Laser Welds

An evaluation of the role continuous wave laser process parameters has on pore formation in milliscale keyhole mode welds is presented

BY J. T. NORRIS, C. V. ROBINO, D. A. HIRSCHFELD, AND M. J. PERRICONE

ABSTRACT

Porosity formation in milliscale partial penetration Nd:YAG laser keyhole mode welds is not well understood. Prior investigations of weld porosity examining the relationship between process parameters and laser keyhole stability have largely been qualitative and mostly focused on welds outside the milliscale regime with a penetration in excess of 2 mm. Little characterization of milliscale keyhole regime welds, ubiquitous in dense miniature packaging, has been performed and as a result, very limited design guidance is available for manufacturing of such components. The present study utilizes a systematic evaluation of the role with continuous wave (CW) laser process parameters on pore formation in milliscale keyhole mode welds. Parameters investigated include laser output power, weld speed, and beam size. Porosity characteristics were obtained through X-ray radiography and contrasted to metallographic weld analysis and laser process parameters. Results showed distinct trends in pore formation. For CW laser welds, the average pore size was found to increase linearly with the weld cross-sectional area and parabolically as a function of heat input. Three porosity types were identified that exhibit unique size, location preference, and frequency. Deeper penetration pore-free welds were achieved by using longer lens focal lengths (larger focused beam size). As a result, a simplified geometric weld model is proposed that correlates laser beam spot size as a function of lens focal length and penetration to the onset of porosity. Process parameter maps have been developed to assist in successful weld development. It is shown that through the use of appropriate process parameters, weld porosity can be greatly reduced, if not fully suppressed, in milliscale Nd:YAG laser keyhole mode welds.

Introduction

Porosity in laser welds has largely been attributed to laser keyhole instabilities in the weld pool. Collapsing of the keyhole is thought to trap a gas pocket creating a void (pore) in the weldment — Fig. 1. The mechanisms that lead to instability are not fully understood as many factors are believed to contribute to the general condition of the keyhole. Factors including weld size, laser output modes (e.g. pulsed, continuous wave [CW], and modulated), material type, and weld joint geometry, all

impact laser keyhole formation and evolution. Given that many variables affect keyhole stability, it is not surprising that many researchers consider porosity formation to be random (Refs. 1–3). Prescribed methods for avoiding this defect are scarce in the literature and tend to focus predominately on large-scale welds, commonly much greater than a 2-mm penetration (Refs. 2, 4). Very little information

KEYWORDS

Porosity
Milliscale
Nd:YAG Laser Keyhole
Mode Welds
Continuous Wave (CW)
Type 304L Stainless Steel

on mitigation tactics for smaller milliscale (<2 mm) laser welds common to dense, miniaturized packaging exists (Refs. 5, 6).

Risk related to weld porosity is not easily quantified as it can result in a loss of weld strength, premature fatigue failure, increased in-service creep, and depending upon the gases trapped inside the pores, reduced corrosion resistance (Ref. 7). Each of these can be detrimental to the component's functionality. The extent to which these weld failures occur depends largely upon application — magnitude and type of loading forces, service environment, expected life, etc. — and the severity of the porosity. Applications that suffer the most as a result of porosity are high-reliability applications such as medical and satellite hardware. Reduced reliability and increased risk imposed by weld porosity cannot be accommodated in these applications. Because these component types are often temperature sensitive due to their dense miniaturized packaging, they require a low-heat input joining process, specifically laser keyhole mode welding. As component designs are driven toward smaller and denser packages, porosity in milliscale welds must be better understood.

The objective of this study is to analyze porosity formation in milliscale continuous seam Nd:YAG laser keyhole mode welds and provide guidance for manufacturing such welds. Efforts focused on closure type welds in 304L austenitic stainless steel and the effect of operating parameters, specifically laser output power, weld speed, and lens focal length (or spot size).

Experimental Setup

A Rofin-Sinar Nd:YAG laser, Model CW 015 HQ, and a GSI Lumonics Nd:YAG laser, Model JK802, were used to produce sharp-focus, standing-edge welds on hot rolled 304L stainless steel sheets 1.27 mm thick — Fig. 2. Both lasers

J. T. NORRIS (jnorris@sandia.gov) and D. A. HIRSCHFELD are with the New Mexico Institute of Mining and Technology, Socorro, N.Mex. C. V. ROBINO is with Sandia National Laboratories, Albuquerque, N.Mex. M. J. PERRICONE, formerly with Sandia National Laboratories, is currently with R. J. Lee Group, Monroeville, Pa.

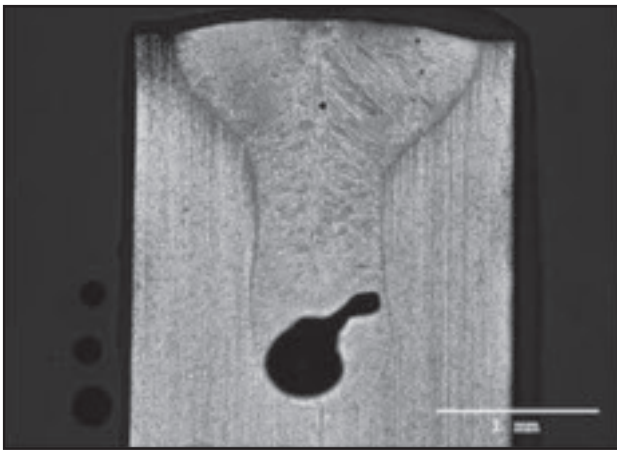


Fig. 1 — Common Nd:YAG laser beam weld porosity. A transverse metallographic cross section exposing an irregularly shaped pore (~0.5-mm-diameter dark region) formed at the base (root) of the weld.

were flash lamp driven and fiber delivered. Weld sample composition (in wt-%) was 0.03% C, 18.09% Cr, 0.2% Cu, 1.73% Mn, 0.16% Mo, 0.06% N, 8.57% Ni, 0.36% Si, 0.024% P, and 0.001% S. Weld samples were dimensioned to 100 × 25.4 × 1.27 mm with a weld length of 89 mm. In order to minimize deformation for optimum part fitup and maintain square joint corners, weld samples were electric discharge machined (EDM) and lightly machine finished along the long edge to remove any EDM wire deposit. Prior to welding, all samples were ultrasonically cleaned in isopropyl alcohol.

The average laser power was measured prior to each test set using either an Ophir Nova II meter with a 1000-W thermal head detector or Macken Instruments P2000 laser power probe. The average power ranged from 300 to 1200 W at travel speeds from 13 to 51 mm/s with a spot size of 200 to 500 μm. Spot size was measured with a Promotec Laser Scope UFF100. All welds were made at a sharp focus using 80-, 120-, 160-, and 200-mm lens focal lengths. Ultrahigh purity (UHP) argon shielding gas was delivered with a side shield nozzle trailing the weld pool (Rofin-Sinar welds) or coaxially (GSI Lumonics welds) at flow rates of ~33 standard L/min. Weld porosity was quantified by postweld X-ray radiography using an AXI Viscom Micro Focus X-ray at 120 kV and 100 μA.

X-ray radiography was used to characterize porosity throughout the fusion zone. The standing edge joint geometry allowed for a “side-to-side” X-ray of the sample resulting in images that reduce pore volume to a two-dimensional projection relative to the weld penetration — Fig. 3. Top-down X-rays revealing pore locations along the weld width were not taken because small pores would not appear due to the height of the samples. Therefore, differentiating individual

pores within the same plane relative to the weld width was not possible. As a result, some pores may appear irregular in shape or oversized, and thus limits the pore analysis to the approximation of pore diameter, location, and frequency (relative to the weld penetration).

While some inference of pore location relative to width may be obtained from metallographic transverse cross sections, this information is not believed to be critical to the pore analysis. Due to the restricted contrast between the pores and surrounding material, pore diameter resolution was limited to 0.13 mm. Pores measuring less than 0.13 mm diameter and comparatively rare in occurrence were defined as micro pores, pore free, or having a diameter of 0.075 mm (one-half the pore diameter resolution) for the purpose of graphical analysis. For each weld sample, the average pore diameter was determined by superimposing multiple line segments (25 mm in length) over a region of porosity, measuring the width of each pore intersecting the line, and then calculating an average diameter. This ensured that all pore sizes were accounted for despite considerable differences in contrast.

By multiplying the number of pores within a line segment with the weld speed, the frequency of pore formation could be determined. Attempts were made to use automated image analysis software to determine the pore characteristics, but it was unsuccessful due to large contrast variations between pores. The result was undetected or undersized pores, the extent of

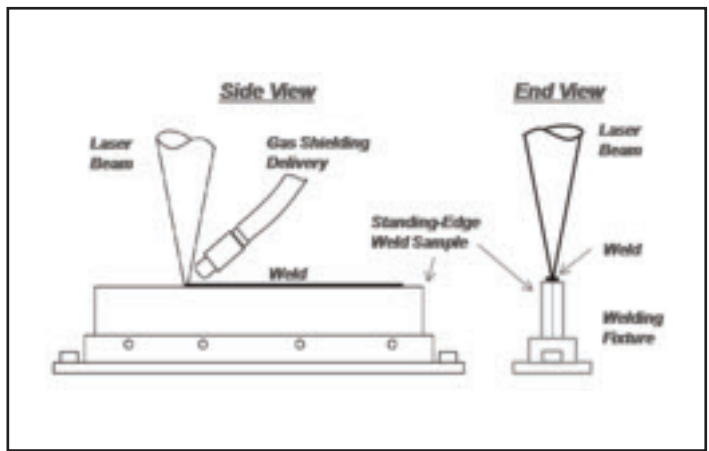


Fig. 2 — Weld setup schematic. Weld joint consists of two side-butt flat plates. The laser is focused at the top of the sample and centered on the weld joint. Welds made with the Rofin laser used trailing side nozzle gas shielding (as shown above). Welds made with the Lumonics laser used coaxial shielding along the beam path (not shown).

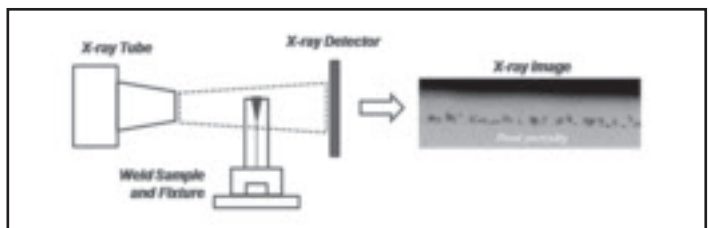


Fig. 3 — X-ray radiography schematic. X-ray image taken through the weld joint.

which varied between samples.

Longitudinal and transverse metallographic cross sections were made to allow the assessment of weld penetration, width, and cross-sectional area. Three to four transverse sections, chosen randomly along the length of the weld, were made per weld sample.

Results and Discussion

Identification of CW Porosity Types

Analysis of the CW welds revealed three types of porosity that can be qualitatively described as uniform, transitional, and root. Uniform porosity appears to have an even distribution throughout the fusion zone of small-diameter pores generally less than 0.25 mm — Fig. 4A. This type of porosity was only observed at high-weld velocities (i.e., 34 mm/s). Root porosity, often referred to as linear porosity (Ref. 8), predominately forms at the root of the weld, appears relatively consistent in size (for a fixed weld parameter), forms at a perceived frequency, and coincides with lower travel speeds — Fig. 4C. This episodic formation implies that keyhole collapse likely occurs at a regular frequency. Transitional porosity exhibited characteristics of both root and uniform porosity containing periodic

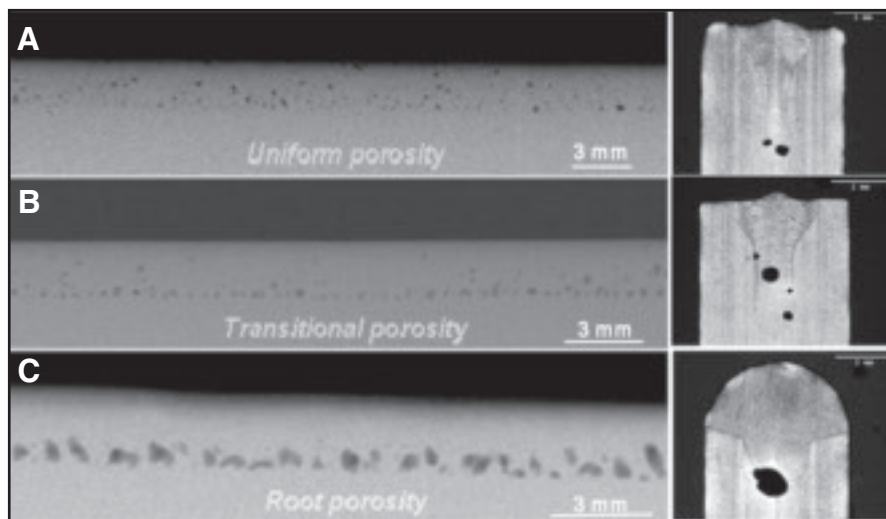


Fig. 4 — X-ray radiographs and micrographs illustrating uniform (A), transitional (B), and root porosity (C) in argon shielded sharp focus CW laser beam welds. A — 34 J/mm, 2.3-mm penetration, 0.18 mm average pore diameter; B — 42 J/mm, 2.2-mm penetration, 0.25 mm average pore diameter; C — 55 J/mm, 2.2-mm penetration, 0.43 mm average pore diameter.

medium size pores at the root and smaller pores distributed throughout the fusion zone — Fig. 4B. This porosity type appeared at intermediate weld speeds. The corresponding micrographs for each porosity type show the effect process parameters have on weld shape and likely the type of porosity formed. All porosity types measured considerable variation around the average pore diameter value but generally had a standard error of 0.03 mm or less. These trends in CW weld porosity suggest that porosity is not as random as was expected for milliscale welds (Refs. 3, 9, 10).

Effects of CW Power and Travel Speed

A broad range of welding parameters for the 120-mm focal length lens was evaluated in this study. This range produced welds of various sizes, shapes, and penetrations all meeting the constraint of a milliscale weld. An analysis of these welds revealed that increasing travel speed decreases the nominal pore size for a given penetration, and that welds having comparable depths can be produced with considerably different pore and weld attributes. Examination of the 120-mm lens data set welded with UHP argon yielded a penetration-porosity map, Fig. 5, where weld depth and average pore size were examined as a function of CW power and travel speed. Well-behaved trends in penetration and average pore size are seen for the milliscale keyhole mode welds in the range examined.

Figure 5 shows solid and dashed lines corresponding to penetration and average pore size, respectively, as a function of CW power. Each line is color coded with respect to travel speed. It is apparent in the diagram that as weld speed increases,

moving from upper left to lower right, average pore diameter decreases.

For example, weld A of Fig. 5 shows a keyhole mode weld with a 1.1 aspect ratio (depth to width) made at 13 mm/s and 575 W (44 J/mm heat input). These parameters yielded root porosity with a nominal pore diameter of 0.25 mm. In contrast, weld B, also a keyhole mode weld but having a greater aspect ratio (1.7) and made at 34 mm/s and 935 W (27 J/mm heat input), resulted in uniform porosity with a nominal pore size of 0.14 mm. The resulting size and shape of these welds is indicative of the unique heat flow patterns occurring in each part and as it is suggested by these data, exhibit distinct pore formation susceptibilities. The combination of power and speed that produced weld A resulted in more severe, larger-diameter pores. Both weld A and B have similar penetration (1.7 and 1.9 mm, respectively) but have considerably different heat inputs (44 vs. 27 J/mm, respectively). [Note, weld penetration is measured from the root of the weld to the original weld sample surface.

To understand the mechanisms driving porosity formation and for developing methods to avoid its occurrence, characterization of process parameter effects on the direction of heat flow in the part (i.e., 2D, 2.5D, 3D) resulting in welds of various sizes and shapes is necessary. As shown in Fig. 5, weld A and B have comparable penetration depths but differ in weld size and shape, and show different susceptibilities to weld porosity formation. As will be established, these differences relate to the heat input associated with each set of welding parameters; in this case, 44 and 27 J/mm, respectively. The combination of power and speed producing weld A

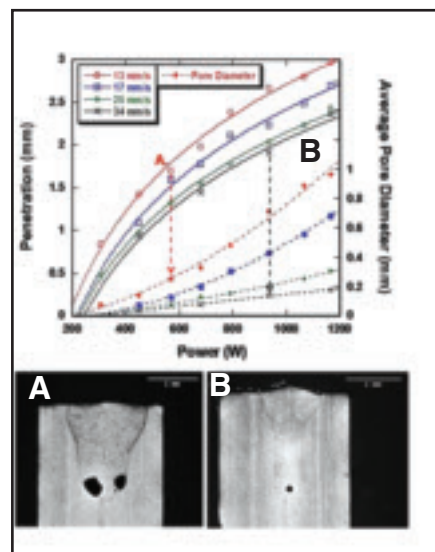


Fig. 5 — Penetration and pore size vs. CW power for Ar-shielded focus CW laser beam welds with 120-mm lens, power of 250–1200 W, speeds of 13–34 mm/s. Transverse micrographs of two welds with similar penetration are as follows: A — 13 mm/s 575 W with 1.7-mm penetration and 0.25 mm nominal diameter root type pores; and B — 34 mm/s 935 W with 1.9-mm penetration and 0.14 mm nominal diameter uniform type pores. Average pore diameter generally had a standard error of 0.03 mm or less.

yielded increased lateral melting (increasing weld cross-sectional area) without the benefit of increased penetration.

In Fig. 6, the effect of lateral melting (weld size) to pore size is more closely examined. In agreement with what might intuitively be expected, pore size increases with increasing weld size. Perhaps less intuitive, however, is the observation that average pore diameter increases linearly with weld cross-sectional area (proportional to weld volume per unit length). The implication is that for a given weld penetration (for this weld type and laser mode), increased lateral melting directly increases pore formation susceptibility. These data also illustrate the importance of molten weld pool inertial forces on keyhole stability. In a keyhole mode weld, vapor pressure recoil displaces the molten material, and in this way increases the penetration depth (Refs. 3, 11–13). Once penetration and the vapor recoil force are maximized, continued melting of the surrounding metal increases the molten layer surrounding the keyhole. In turn, a higher vapor force is then needed to counter the increased molten volume, but because beam irradiance is relatively constant, the vapor recoil force of the fully developed keyhole is fixed (exhibits an upper threshold specific to the process parameters used). The molten material eventually overcomes the vapor force and collapses the keyhole.

A similar argument has been proposed for keyhole collapse in deep penetration

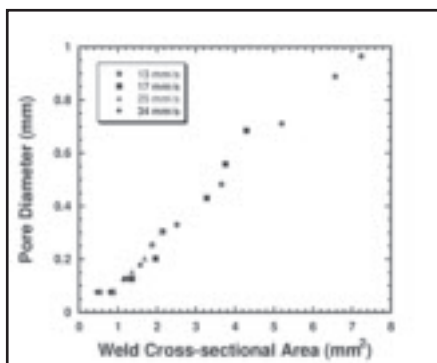


Fig. 6 — Average pore diameter vs. weld area for argon-shielded sharp focus CW laser beam welds made with a 120-mm lens. Power and weld speed varied from 250 to 1200 W and 13 to 34 mm/s, respectively.

CO₂ laser welds (Ref. 14). The increased melting that occurs near the surface in a CO₂ weld due to the high-temperature plasma, which gives the CO₂ weld its nail-head appearance, results in a condition where the vapor pressure is inadequate to maintain a stable keyhole. In turn, the keyhole is collapsed by the localized surface melting and a root type pore is formed. Excessive (lateral) melting appears to result in keyhole instabilities in both milliscale and deep penetration nail-head shaped welds, and these instabilities, in turn, result in the formation of porosity.

The results of Figs. 5 and 6 demonstrate the effect lateral melting has on pore formation and minimized porosity size (for a given penetration) requires process parameters that yield small area high aspect ratio welds. In a CW mode weld, this is largely achieved by increased travel speed.

Quantitatively illustrated in Figs. 5 and 6 is the advantage of small area high aspect ratio welds where minimum heat input is used to achieve the desired weld penetration. From an engineering standpoint then, a reasonable way to quantify effective melting along the joint is by the weld penetration efficiency (η_p) or the depth of penetration per unit of linear heat input. By reducing weld volume through decreases in heat input, pore size is minimized as well as weld temperature and distortion in the part. These observations hold particular significance for heat-sensitive parts where the pursuit of a high penetration efficiency operating space is crucial for optimal weld development. This figure of merit, weld penetration efficiency, allows for welds of varying power and speeds to be characterized and compared, and for the welding process to be optimized in a quantifiable sense relative to design requirements (i.e., penetration). Weld A of Fig. 5 has a weld penetration efficiency of 0.04 mm/J/mm while that of weld B is 0.07 mm/J/mm.

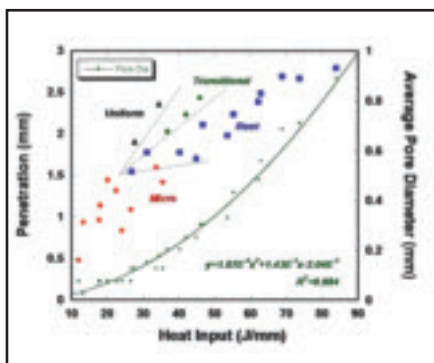


Fig. 7 — Porosity type characterized by weld depth and heat input for focused argon-shielded CW laser beam welds made with a 120-mm lens. Average pore diameter is described as a parabolic function of heat input irrespective of porosity type. Power and weld speed varied from 250 to 1200 W and 13 to 34 mm/s, respectively.

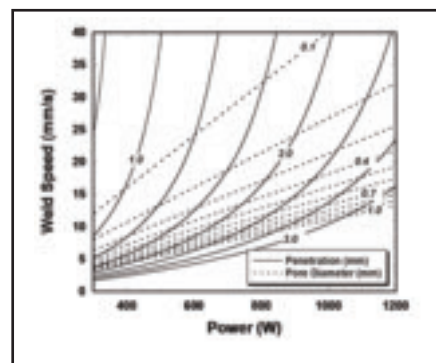
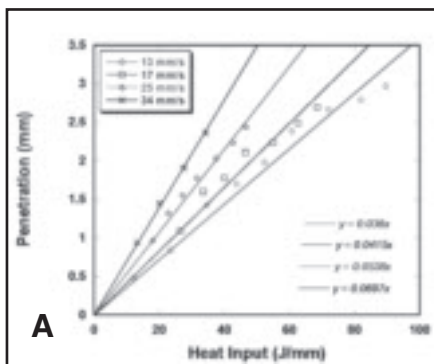
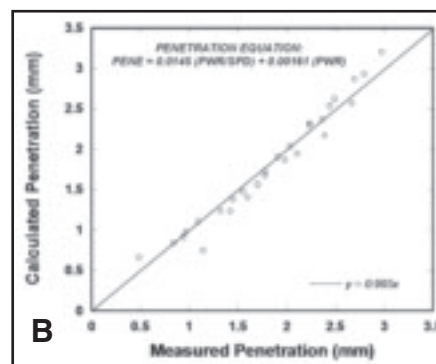


Fig. 8 — Process map showing the effects of power and speed on penetration and pore diameter for focused argon-shielded CW laser beam welds made with a 120-mm lens. Power and weld speed varied from 250 to 1200 W and 13 to 34 mm/s, respectively.

Fig. 9 — A — Linear fit of penetration as a function of heat input and travel speed; B — Comparison of calculated and measured penetration values for focused argon-shielded CW laser beam welds made with a 120-mm lens. Power and weld speed varied from 250 to 1200 W and 13 to 34 mm/s, respectively.



Evaluation of Porosity Types Relative to Process Parameters

Further analysis of the 120-mm lens data set welded under UHP argon identified that linear heat input (laser output power divided by the weld speed) can be used to predict the nominal pore size observed in this weld type. This combines the individual effects of power and speed, and allows for a more general evaluation of weld parameters to nominal pore size and penetration depth. Evaluating pore size as a function of heat input also revealed that porosity types readily segregated into distinct operating regimes.

In Fig. 7, penetration depth and nominal pore size for the 120-mm data set are plotted as a function of heat input. Representative lines are drawn to distinguish between regions of porosity type. The slope of each line represents penetration efficiency that increases with the increasing slope of the line. In this plot, weld speed is effectively decreasing from left to right. It was observed that for constant weld speeds, the tendency to form pores changes from none or micro porosity to either root, transitional, or uniform porosity

with increasing power (and therefore heat input). As an example, welds made at high weld speeds (e.g., 34 mm/s) yielded high aspect ratio (high penetration efficiency) keyhole mode welds that exhibited a shift from micro porosity to uniform porosity as power increased. Large root pores were not observed in these welds and only minimal lateral melting occurred.

In contrast, welds made at much slower weld speeds (e.g., 13 mm/s) displayed lower penetration efficiency with a lower aspect ratio and increased lateral melting. Porosity transitioned from micro porosity to large root porosity with increasing power. This is because weld volume increases with the increased heat input of the lower travel speed welds and, as has already been shown in Fig. 6, average pore diameter increases with increased weld cross-sectional area.

Further analysis of these data reveals a strong correlation between linear heat input and nominal pore size. Irrespective of weld speed, the nominal pore size was found to increase with heat input. The green parabolic curve of Fig. 7 shows that all discrete porosity types reduce to a single curve. A single point on the curve rep-

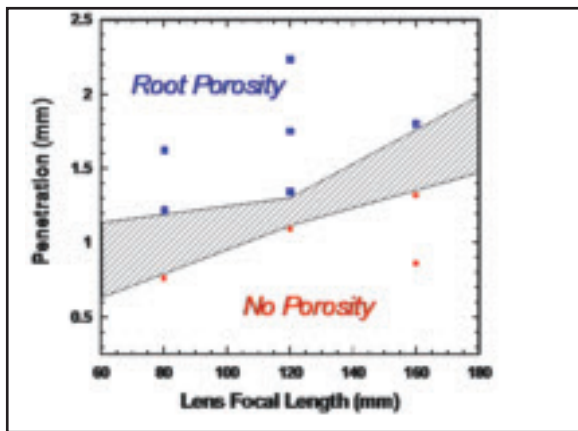


Fig. 10 — The effect of lens focal length on the onset of porosity relative to weld depth. The transition region from no porosity to root porosity is denoted by the cross-hatched area. All welds were made at focus with argon shielding. The CW power varied from 250 to 1000 W at a weld speed of 17 mm/s, respectively.

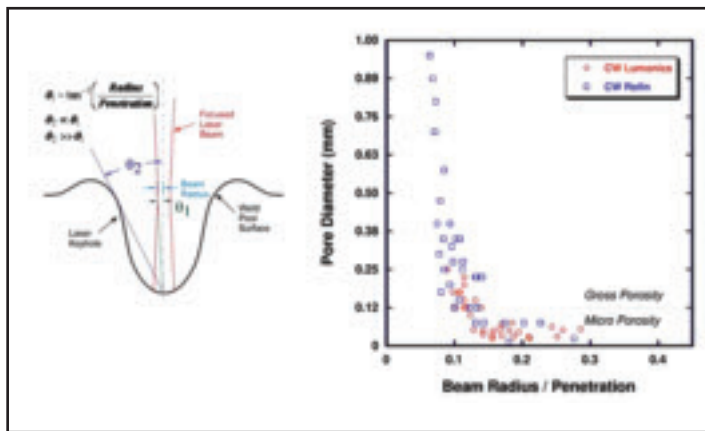


Fig. 11 — Schematic of the liquid-vapor surface produced during keyhole welding. The relative angles formed between the beam radius and penetration (θ_1), and keyhole hole opening size and penetration (θ_2) are denoted. The plot identifies porosity onset as a function of beam radius and penetration depth. Both Rofin and Lumonics welds are presented with lens focal lengths from 80 to 200 mm (spot radius from 120 to 240 μm). All welds were made with argon shielding at focus. The CW power and weld speed varied from 120 to 1200 W and 13 to 51 mm/s, respectively.

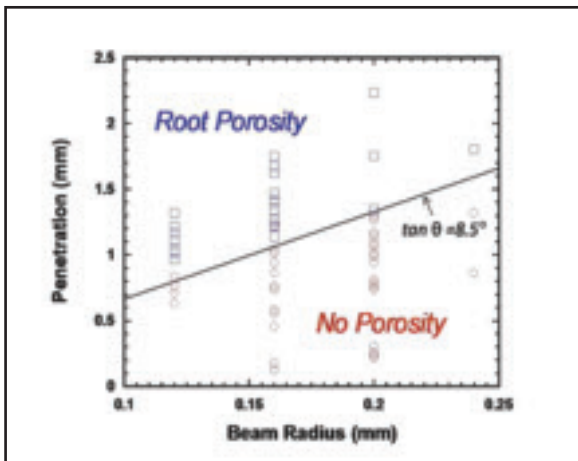


Fig. 12 — Plot verifying the porosity onset model of Fig. 11. Line corresponds to a beam radius/penetration ratio of 0.15 or a θ_1 angle of 8.5 deg. Both Rofin and Lumonics welds are presented with lens focal lengths from 80 to 200 mm (spot radius from 120 to 240 μm). All welds were made with argon shielding at focus. The CW power and weld speed varied from 120 to 1200 W and 13 to 51 mm/s, respectively.

representing a constant nominal pore size and heat input corresponds to multiple penetration depths of varying pore types. Therefore, nominal pore diameter for this weld type is a function of operator-defined heat input, and by minimizing this quantity, pore size is reduced. The parabolic rise of the curve illustrates how rapidly pore size increases with increasing heat input. To minimize weld porosity, heat input must be low and penetration efficiency high.

Empirically Determined Process Map for CW Milliscale Welds

Given the well-behaved nature of penetration and average pore diameter relative to CW power and speed, a process map specific to these data was developed and is pre-

sented in Fig. 8. It shows the general trends in penetration and pore size relative to CW welding parameters for milliscale keyhole mode welds. Penetration as a function of power and speed is denoted by the solid lines and pore diameter is denoted by the dashed lines. As shown in Fig. 5, increased weld speed yields decreased pore size and so it is in Fig. 8, where only small-diameter pores are noted near the top of the graph. Also identified was the role of heat input in Fig. 7. High heat inputs were shown to result in large-diameter pores. As heat input increases from upper-left to lower-right, so does pore size. These contours were determined using a parabolic curve fit of data shown in Fig. 7. The combined effects of power

and speed on penetration are noted by the upward sloping contours of the solid curves. Empirically, penetration can be described as a function of heat input and power by the following equation.

$$Penetration = 0.015 \left(\frac{Power}{Speed} \right) + 0.0016 (Power) \quad (1)$$

In general, the relationship between penetration and heat input is complex, and can be affected by factors such as keyhole mode, joint geometry, and the character of heat flow. Over the penetration range investigated here, however, and for constant travel speeds, penetration was found to change linearly with heat input — Fig. 9A. The size and shape of the weld,

for a given material type and joint geometry, are largely controlled by the power transfer and melting efficiencies. These are functions of the delivered laser power and exposure time (Refs. 8, 15, 16), which are represented in Equation 1 as the process parameters power and speed. The use of these parameters to identify weld penetration, therefore, seems logical. A comparison between the calculated and measured penetration values, determined by Equation 1, is presented in Fig. 9B. For weld depths up to 3 mm, the penetration equation (Equation 1) shows good agreement to measured values.

Lens Focal Length Effects on Porosity

To identify the effect of lens focal length on pore formation, additional tests were conducted using 80- and 160-mm lenses with power varying from 300 to 1200 W and a constant weld speed of 17 mm/s. Just as the 120-mm lens transitioned from micro porosity to root porosity with increasing penetration, the same was found for the 80- and 160-mm lenses. It was found that the onset of porosity occurred at the shallowest penetration when using the 80 mm, or shortest, focal length lens and by increasing focal length, penetration was increased before the onset of porosity. This is shown in Fig. 10 where penetration is plotted as a function of lens focal length. Regions of porous and pore-free welds are designated. The 80-mm lens began forming pores between 0.75- and 1.20-mm penetration. Welds produced using the 160-mm lens did not begin forming pores until penetration reached 1.30–1.80 mm. The porosity onset region is marked by the cross-hatched area.

To better understand the observed effect of spot size (lens focal length) on porosity formation, a schematic relating

keyhole opening (diameter), laser beam diameter, and keyhole depth is presented in Fig. 11. This depiction is adapted, and is similar to those obtained from, high-speed X-ray imaging studies (Ref. 1) and simplified numerical solutions of keyhole phenomenon (Refs. 17–19). The drawing was not generated to scale but is adequate for the following discussion. As has been described by a number of investigators (Refs. 3, 11, 16), as the keyhole depth increases, surface tension and increasing weld pool inertial forces act against the vapor pressure recoil force until a point of instability is reached and the keyhole collapses. Based upon the trends observed in Fig. 10, a relationship between keyhole diameter and weld depth is thought to exist at the point of instability (the onset of porosity).

Theta 2 (θ_2) in the drawing of Fig. 11 describes an angle relating penetration to keyhole opening diameter. Under quasi-stable keyhole conditions, this angle, θ_2 , is assumed to be proportional to the angle formed between the beam radius and depth of penetration, or θ_1 ; as keyhole depth increases, the angle produced decreases. In the graph of Fig. 11, nominal pore diameter is plotted against the quotient of the beam radius and depth of penetration. The arc tangent of the quotient is the angle between the beam radius and keyhole depth (θ_1). Represented in the plot are data for welds made with the Rofin and Lumonics systems with a beam radius ranging from 0.160 to 0.240 mm and 0.120 to 0.200 mm, respectively. It was found that at a quotient (beam radius/penetration) value of ~ 0.15 , gross porosity is initiated and becomes more prevalent with decreasing quotient value. As the angle between the beam diameter and weld depth (θ_1) decreases, keyhole instability in the form of porosity increases. A value of 0.15 corresponds to a keyhole instability angle of 8.5 deg (arc tangent of the radius over the penetration).

In Fig. 12, the CW data for the Rofin and Lumonics lasers are reconstructed in a manner similar to that of Fig. 10, with penetration as a function of spot size (spot size instead of lens focal length) and with a solid line corresponding to a θ_1 angle of 8.5 deg; or an beam radius/penetration ratio of 0.15. The predicted angle of 8.5 deg appears to accurately define the penetration depth at which porosity begins to form. Having incorporated all porosity types produced at various travel speeds, powers, and lens focal lengths for two independent laser welding systems (Rofin and Lumonics lasers), this result supports the geometric model as being reasonable and predictive. It should be noted that the determined shallow angle of 8.5 deg is indicative of the small beam size and much smaller than the actual keyhole opening.

From an application standpoint, the

observed trend in porosity as it relates to focal length is favorable because longer focal length lenses offer both a larger depth of focus for process robustness and a reduced beam angle, decreasing the likelihood of beam clipping in recessed weld applications. The smaller beam angle also allows for side shielding to be positioned closer to the weld, thereby providing better shield gas coverage.

Conclusions

A study of weld porosity specific to milliscale partial penetration laser keyhole welds in Type 304L stainless steel has been conducted to provide design guidance for manufacturing of pore-free laser welds, quantify porosity characteristics, and to obtain a better understanding of the effects of process parameters on keyhole stability and porosity formation. The following conclusions have been drawn:

1. Radiographic analysis of CW mode laser welds revealed three types of porosity (root, transitional, and uniform) depending upon laser process parameters. Low travel speed, high-heat input schedules resulted in root porosity that transitioned to uniform porosity with increasing speed and reduced heat input.
2. Average pore diameter in CW mode welds increases linearly with weld cross-sectional area; small area, high penetration efficiency welds exhibit minimum porosity. This is primarily achieved through higher travel speeds.
3. The average pore size was found to increase parabolically with laser heat input, irrespective of porosity type.
4. Process mapping was used to empirically relate weld depth and nominal pore diameter to laser CW power and weld speed.
5. In CW milliscale welds, utilizing a larger beam diameter by increased lens focal length deferred the onset of porosity allowing for greater penetration depths to be reached without forming pores. For many applications, this is an easily applied method for porosity reduction.
6. An empirical geometric model was proposed correlating porosity formation to laser beam spot size and penetration depth. The model was verified with milliscale welds produced by two independent laser systems (Rofin and Lumonics). The relationship between laser beam spot size and weld depth is a significant factor affecting weld porosity.

Acknowledgments

The authors would like to thank Alice Kilgo in the Metallography Lab for her careful preparation of metallographic samples and Danny MacCallum in the laser lab for his support and contribution toward this project. This work was per-

formed at Sandia National Laboratories, a multiprogram laboratory operated by Sandia Corp., a Lockheed Martin Co., for the United States Department of Energy under contract DE-AC04-94AL85000.

References

1. Naito, Y., Masutani, M., and Katayama, S. 2006. Effect of oxygen in ambient atmosphere on penetration characteristics in single Nd:YAG laser and hybrid welding. *Journal of Laser Applications* 18: 21–27.
2. Matsunawa, A., Kim, J. D., and Katayama, S. 1997. Porosity formation in laser welding — Mechanisms and suppression methods. *LIA 16th ICALEO Conference Proceedings*, 85 Sec G, 73–82.
3. Heiple, C. R., and Burgardt, P. 2005. Fluid flow phenomena during welding. *ASM Handbook #6 — Welding, Brazing, and Soldering*, pp. 19–24.
4. Estill, W. B., and Formisano, B. D. 1983. Porosity decrease in laser welds of stainless steel using plasma control. Sandia Report SAND83-8024. Livermore, Calif.: Sandia National Laboratories.
5. Kuo, T. Y., and Jeng, S. L. 2005. Porosity reduction in Nd:YAG laser welding of stainless steel and Inconel alloy by using a pulsed wave. *J. Phys. D: Appl. Phys.* 38: 722–728.
6. Haboudou, A., Peyre, P., Vannes, A. B., and Peix, G. 2003. Reduction of porosity content generated during Nd:YAG laser welding of A356 and AA5083 aluminum alloys. *Materials Science and Engineering A363*: 40–52.
7. Daugherty, W. L., and Cannell, G. R. 2003. Analysis of porosity associated with Hanford 3013 outer container welds. *Practical Failure Analysis* 3(4): 56–62.
8. Mazumder, J. 2005. Procedure development and practice considerations for laser-beam welding. *ASM Handbook — Welding, Brazing, and Soldering*, pp. 874–880.
9. Mazumder, R. 2005. Laser-beam welding. *ASM Handbook — Welding, Brazing, and Soldering*, pp. 262–269.
10. Overview of weld discontinuities. 2005. *ASM Handbook — Welding, Brazing, and Soldering*, pp. 1073–1080.
11. Fabbro, R., and Chouf, K. 2000. Keyhole modeling during laser welding. *Journal of Appl. Phys.* 87(9): 4075–4083.
12. Solana, P., and Negro, G. 1997. A study of the effects of multiple reflections on the shape of the keyhole in the laser processing of materials. *J. Phys. D: Appl. Phys.* 30: 3216–3222.
13. Messler, R. W. Jr. 1999. *Principles of Welding*. New York, N.Y.: Wiley Interscience.
14. Kim, T. H. 1991. Porosity formation in laser-beam materials processing. *Journal of Mat. Sci. Letters* 10: 400–402.
15. Fuerschbach, P. W. 1996. Measurement and prediction of energy transfer efficiency in laser beam welding. *Welding Journal* 75(1): 24-s to 34-s.
16. Fuerschbach, P. W., and MacCallum, D. O. 1995. Variation of laser energy transfer efficiency with weld pool depth. *LIA 14th ICALEO Conference Proceedings*.
17. Jin, X., Li, L., and Zhang, Y. 2002. A study of fresnel absorption and reflections in the keyhole in deep penetration laser welding. *J. Phys. D: Appl. Phys.* 35: 2304–2310.
18. Semak, V., and Matsunawa, A. 1997. The role of recoil pressure in energy balance during laser materials processing. *J. Phys. D: Appl. Phys.* 30: 2541–2552.
19. Naito, Y., Mizutani, M., Katayama, S., and Bang, H. 2004. Effect of ambient atmosphere on penetration geometry in laser and hybrid welding. *LIA 23rd ICALEO Conference Proceedings*.